A simple and fast method to downscale chemistry transport model output fields from the regional to the urban/district scale

Bertrand Bessagnet, Enrico Pisoni, Alexander de Meij, Laurent Létinois, Philippe Thunis

Environmental Modelling and Software 164 (2023) 105692

Contents lists available at ScienceDirect

Environmental Modelling and Software

journal homepage: www.elsevier.com/locate/envsoft

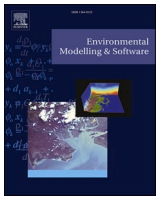

A simple and fast method to downscale chemistry transport model output fields from the regional to the urban/district scale

Bertrand Bessagnet [a,*], Enrico Pisoni [a], Alexander de Meij [b], Laurent Létinois [c], Philippe Thunis [a]

[a] European Commission, Joint Research Centre (JRC), Ispra, Italy
[b] MetClim, Varese, Italy
[c] INERIS, Parc Technologique Alata, BP 2, 60550, Verneuil-en-Halatte, France

ARTICLE INFO

Handling Editor: Daniel P Ames

Keywords:
Modelling
Air quality
Downscaling
Emissions
Inventory

ABSTRACT

For policy applications, the need to improve the resolution of environmental variables is crucial. Air pollution assessment indeed requires the use of air pollutant concentration fields at a high resolution, to better evaluate the exposure of citizens. In this paper, we propose a fast proxy-based downscaling strategy, to downscale air quality modelling results using the fraction of the pollutant concentration influenced by precursor emissions in a given cell. The approach combines in an additive way (i) a classically interpolated background pollutant fraction, with (ii) a proxy-based concentration derived from the emissions. The proxy-based pollutant fraction is spread over the high resolution mesh into the surrounding cells with a Gaussian approach to account for diffusion effects. The evaluation of our approach against observations shows its relevance to create reliable air pollution concentration fields at a higher resolution, starting from a coarse resolution modelling results.

1. Introduction

In its last report of the European Environment Agency, around 25% of the European urban population remains exposed to air quality exceeding the European Union air quality standards, leading to about 400,000 premature deaths yearly (EEA, 2019). To assess air pollutants exposure, identify the sources of pollution and develop strategies to curb air pollution, air quality models are essential tools, expected to be more and more robust and computationally-efficient with time (Denby et al., 2020; Jiang et al., 2020; Mu et al., 2022; Ramacher et al., 2021; Sokhi et al., 2022; Terrenoire et al., 2015). In practice, a chemistry transport model generally operates up to 1 km resolution, sufficient to show the variability of concentrations over large cities in Europe or district levels in Megacities like in China or India, but this resolution is not sufficient for many cities of smaller size. Another challenge of working at finer scale relates to the availability of fine-scale emissions inventories. While the downscaling of large scale emissions using proxy (*e.g.* population, road, large point sources data) approaches as done in the several model pre-processing (Binkowski and Roselle, 2003; Menut et al., 2021; Ramacher et al., 2021) is a solution, this remains a first guess estimate.

Modelling outputs statistics (MOS) techniques are common methods to adapt CTM outputs to observations and remove the model bias, based on functions of diagnostic variables like meteorological data. These methods based on kriging algorithms have been used for air pollution operational forecasting (Beauchamp et al., 2017, 2018; Malherbe et al., 2014). These methods can associate ancillary variables like emissions inventories to better reallocate the concentrations of primary pollutants. However, applying kriging methods can still take several minutes to hours on a single processor to generate high-resolution maps over large regions. This method is not adapted to online uses or to Personal Computers. Recently (Denby et al., 2020; Mu et al., 2022), have developed a proxy based downscaling approach for the EMEP model.

Currently, statistical methods using deep-learning approach (LeCun et al., 2015) based on Convolutional Neural Network (CNN) architectures can provide a framework to perform quick high-resolution simulations (Bessagnet et al., 2019, 2021; Dong et al., 2014; Sorek-Hamer et al., 2022; Xing et al., 2020). These methods capture the main patterns, as a complex model would do while keeping a sufficient accuracy. These methods remain however complex to design and improvements are needed to better account for the long-range transport of pollutants and

Abbreviations: CLC, Corine Land Cover; CNN, Convolutional Neural Network; CTM, Chemistry Transport Model; GNFR, Gridding Nomenclature For Reporting; HR, High Resolution; HRG, High Resolution Grid; LR, Low Resolution; LRG, Low Resolution Grid; MOS, Model Output Statistic; MQI, Model Quality Indicator; PM, Particulate Matter; PM10, PM with diameter below 10 μm; PM2.5, PM with diameter below 2.5 μm; RMSE, Root Mean Square Error.

* Corresponding author.
E-mail address: bertrand.bessagnet@ec.europa.eu (B. Bessagnet).

https://doi.org/10.1016/j.envsoft.2023.105692
Received 7 December 2022; Received in revised form 29 March 2023; Accepted 29 March 2023
Available online 3 April 2023

chemical processes.

In this study, we present a fast alternative methodology to downscale low-resolution (LR) simulation outputs to higher resolution (HR). Compared to the approach developed for EMEP as in (Mu et al., 2022) this approach can be used to any model outputs and account for meteorological parameters to better calibrate the Gaussian kernel parameters. An application and an evaluation of the methodology is provided. Our application focus on NO_2, $PM_{2.5}$ and PM_{10} concentrations.

2. The downscaling methodology

2.1. The method

The objective is to downscale the 2D air pollutant concentrations of the CTM output fields to a finer grid with a given longitude and latitude scale ratio. This methodology can be applied to any air quality models. The principle of our method is described in the following text, together with the required assumptions and more detailed in appendix A.1 and A.2 with a glossary of all variables.

The basis is to define a high-resolution grid (HRG) as a subgrid matching the low-resolution grid (LRG) with a constant scale ratio all over the domain. In our case, the LRG covers Europe at $0.1^\circ \times 0.1^\circ$ and we use a scale ratio in longitude and latitude of 10 to 1 to get a HRG at $0.01^\circ \times 0.01^\circ$ resolution.

We split the pollutant concentration into two main fractions. One that results from longer time-scale processes and is not impacted by emissions at coarse resolutions and the second that is governed by faster time-scale processes and is strongly dependent on local emissions. For particulate matter, this distinction is coherent with the split between primary and secondary fractions as well as natural sources. The detailed description of this split is provided in Equation (3) of Appendix A. The secondary fraction of pollutants shows in general smooth patterns compared to the primary fraction (Paolella et al., 2018; Schaap et al., 2015) but more rigorously the patterns would depend on the wind speed and the grid cell size. There is also a limit for the fine scale resolution, where CTMs applies parameterisations which not solve the processes at the appropriate resolution. This limit depends on the way the CTM parameterize these sub-grid processes. For instance (Lin et al., 2022), show a large increase of the secondary fraction close to roads due to fast chemical processes using CFD (Computational Fluid Dynamic) models. However, to refine the calculation, the second fraction related to the primary emission can be split into two fractions since primary species are also affected by regional transport and natural emissions. Therefore, a resulting split into three fractions is considered as (i) non-primary fraction, (ii) long range primary fraction and (iii) local primary fraction.

The sequence of the algorithm can be summarized as follows (see appendix A.1 and A.2 for mathematical details and particularly Fig. A1). For a coarse cell pollutant concentration C, a percentage Γ of the primary fraction which is directly influenced by a primary precursor is rescaled using proxy data representative of each emission activity sector over the HRG, and then diffused using a Gaussian filtering approach according to a methodology described later. The remaining concentration fraction, composed of the part of primary dominated by transport, and the non primary fraction made of secondary species and including also the natural fraction, is interpolated from the LRG to the HRG and added to the primary fraction diffused by the previous Gaussian approach.

Each pollutant is associated to a precursor: nitrogen oxides ($NOx = NO + NO_2$) for nitrogen dioxides (NO_2), PPM10 for the primary fraction of PM_{10} and PPM2.5 for the primary fraction of $PM_{2.5}$. The downscaled proxy-based concentrations is proportional to the ratio χ of the fine (HRG) to the mother coarse mesh (LRG) emissions of the precursor (Equation (3) of Appendix A1). This step aims at reallocating the load of precursor over the fine emissions grid. A minimum value, set as the minimum obtained over all coarse interpolated concentrations is fixed to avoid zero values.

Two cases exist to evaluate the proxy-based concentrations:

(1) we have access to a fine grid emission inventory and this ratio χ is directly computed on the basis of the HRG emission inventory, the proxy is simply the fine scale emission inventory;
(2) only the LRG emissions are available and a preliminary downscaling of the emission inventory is required using adequate activity specific proxies.

If the emission ratio χ requires the use of proxy to downscale the LR emission inventory (as it is the case in our application), we must first

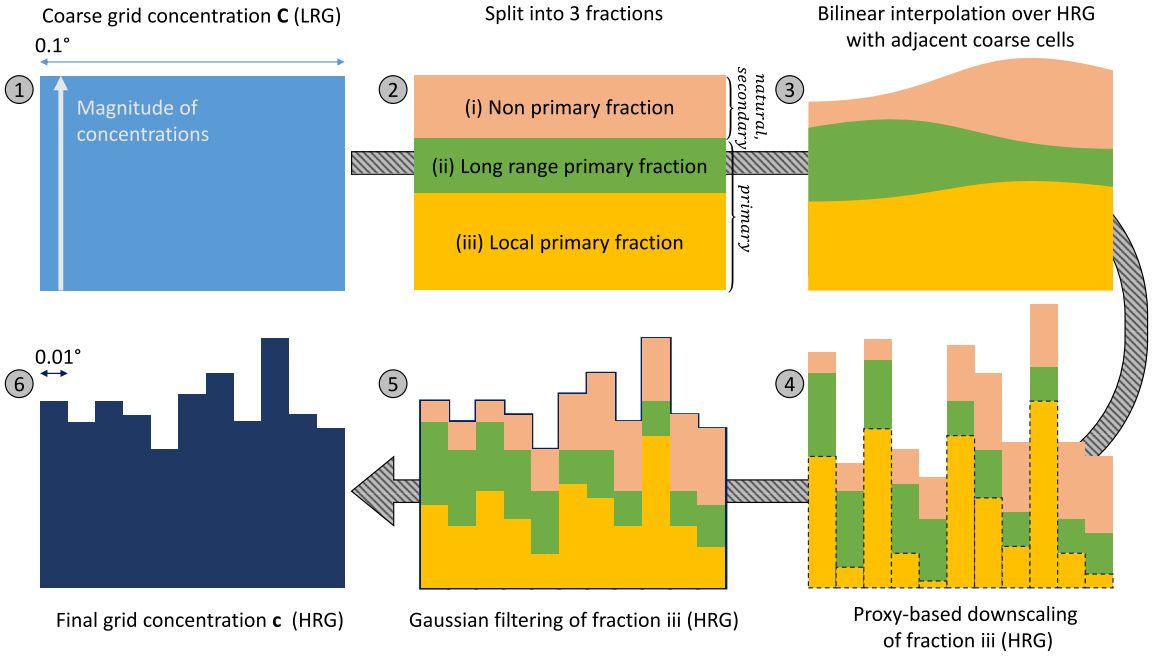

Fig. 1. Visual description of the downscaling methodology in six steps at the coarse cell level (LRG) to downscale a coarse grid LRG concentration field to a finer mesh HRG (e.g. from a 0.1° to a 0.01° grid resolution here).

calculate an activity specific proxy defined as the ratio between its HR value and the sum of all values within a mother coarse grid. Actually, any positive number can be assigned to this ratio as it is normalized by the coarse grid sum. If the sum is equal to zero we assign a uniform value: e.g. 0.01 if 100 fine grid cells are present in the coarse grid cell. This method is fully conservative, in the sense that the average of the fine resolution equals the coarse value.

Afterwards, a multi-gaussian filtering technique (See Appendix A.2) is applied to diffuse the downscaled concentrations according to the annual mean meteorological conditions for the given cell. The vertical diffusion (k) and the 10 m wind speed (u) do mostly govern the dispersion in our modelling strategy through the product $k \times u$, the higher this product is, the higher is the dispersion corresponding to high sigma value in the Gaussian filters. This product ranges from 10 to 150 $m^3\ s^{-1}$ on annual average across the domain from overland surfaces (close to the Alps) to coastal and ocean areas in our example presented later. It is important to note that the wind direction is not taken into account, we consider an isotropic Gaussian dispersion.

The scheme in Fig. 1 displays the downscaling procedure for a regular coarse grid cell of 0.1° resolution downscaled with a scaling factor of 10, therefore to a fine mesh of 0.01° resolution. Fig. A1 in appendix provides a more detailed visualization in 2D of the downscaling procedure.

2.2. Required data

The proposed method requires first, the annual concentrations output fields and associated precursor emissions on a regular grid (LRG) from a chemistry transport model (Bessagnet et al., 2016; Binkowski and Roselle, 2003; Ciarelli et al., 2017; Menut et al., 2021; Simpson et al., 2012). From the LRG, we define a HRG grid using a constant scaling factor to create a HRG that matches exactly the LRG. For instance, a 0.10° × 0.10° resolution grid is downscaled to 0.01° × 0.01° with a scaling factor of 10 in both directions. Two meteorological variables, the wind speed and the vertical diffusion coefficient must also be stored over the LRG grid and interpolated over the HRG grid to calculate the dispersion coefficient (σ) applied in the Gaussian filtering approach.

Second, because a fine scale emission inventory is not available in our application we use a HRG proxy database to refine the emissions. In our work, nine proxies differentiate the main activity sectors, based on databases described hereafter (Table 1). The Corine Land Cover - CLC (for 2018) is one of the datasets produced within the frame of the Copernicus Land Monitoring Service referring to land cover/land use status. CLC provides consistent and thematically detailed information on land cover (*e.g.* industry, off-road, aviation, harbours, etc.) and land cover changes across Europe at 100 × 100 m resolution (CLC, 2020; Feranec et al., 2016). The CLC *tiff* file for 2018 (freely available (CLC, 2020) is pre-processed with GDAL (GDAL, 2022) procedures using an aggregating method based on the median to create *ind*, *off*, *avi* and *har* proxies over the HRG. Indeed, to downgrade the proxy (that has a higher resolution than 0.01°) over the 0.01° grid from the 100 m resolution database, we select the value which appears most often of all the sampled points at 100 m resolution in the 0.01° grid. The USGS (US Geophysical Survey) world land cover database at 30 s arc (Broxton et al., 2014) is used to reallocate agricultural and anthropogenic emissions (*cro* and *art*). The population density at 30 s arc from the Gridded Population of the Word project (CIESIN, 2018) is used to create a population density data (*pop*) and a residential emission proxy (*res*) based on (Terrenoire et al., 2015), this proxy being a function of the logarithm of the population density. The traffic proxy (*tra)* is a mix of a road database identifying the major roads complemented by the population density to identify the urban areas as explained in (Mailler et al., 2017). A proxy derived from the CLC database can only provide an information over the main European countries, therefore for other countries like Ukraine, Russia, North African countries, the information will be missing and no downscaling will be possible over these zones.

Table 1
List of proxies and description.

Name of Proxy φ	Description
ind	Industrial sites: Industrial or commercial units, Port areas, Road areas, Road, Railways, Mineral extraction sites
avi	Aviation: Airport areas
off	Off-road: Construction sites, Port areas, Road areas, Road, Railways, Mineral extraction sites
har	Harbours: Port areas
tra	Traffic: Roads and urbanized areas (based on population density)
res	Residential: Proxy based on population density
pop	Population: population density
cro	Agricultural areas: crops, grasslands, meadow
art	Impervious/Artificial areas

3. Application of the method

Our test case aims at creating HR concentration maps for NO_2, PM_{10} and $PM_{2.5}$ from a CTM simulation at LR for the year 2015. The LR domain extends from 15.05° W to 36.95° E longitude and from 30.05° N to 71.45° N latitude (grid centres) with a horizontal resolution of 0.1° × 0.1° (therefore 521 × 415 grid cells). The final HR Grid rigorously covers the same area at 0.01° × 0.01° resolution (therefore 5210 × 4150 grid cells).

3.1. Generation of CTM outputs

In this study the EMEP off-line regional transport chemistry model version rv_34 (Simpson et al., 2012) is used to analyse the relationship between air pollutant emissions and concentrations over Europe. The vertical structure has 20 levels, with the first located around 50 m. The EMEP model is fed with raw meteorological fields from the European Centre for Medium Range Weather Forecasting (ECMWF-IFS) for the meteorological year 2015 (Owens and Hewson, 2018). The temporal resolution of the meteorological input data is daily, with 3-h time step. The meteorological fields are retrieved on a 0.1° × 0.1° longitude latitude coordinate projection. Vertically, the 60 eta levels IFS fields are interpolated onto the 20 EMEP sigma levels. The MARS equilibrium module is used to calculate the partitioning between gas and fine-mode aerosol phase in the system of inorganics species sulfate/nitrate/ammonium (Binkowski and Shankar, 1995). More information on the gas and aerosol partitioning, meteorological driver, land cover, model physics and chemistry are given in (Simpson et al., 2012). The EMEP emission dataset (Mareckova et al., 2019) at 0.1° resolution is used with a GNFR (Gridding Nomenclature for Reporting) level 1 breakdown (CEIP, 2019). Emissions vertically redistributed by activity sector according to (Bieser et al., 2011; Simpson et al., 2012). The simulation grid is a subset of the EMEP grid (perfect coincidence of grid cell centres) to avoid undesirable spatial interpolations which could lead to some discrepancies.

Yearly annual concentrations are provided for $PM_{2.5}$, PM_{10} and NO_2 over the LRG of 0.1° × 0.1° together with the annual emissions totals detailed by GNFR sectors. To apply the downscaling methodology we use the association between the GNFR activity sector and proxy as in Table 2. Only the surface emissions below 184 m according to the vertical distribution developed by (Bieser et al., 2011) classically used in CTM, this fraction is reported in Table 2.

3.2. Evaluation of the downscaling method

The AIRBASE dataset (AIRBASE, 2022) is used to evaluate the performance of the downscaling for the annual averages of NO_2, $PM_{2.5}$ and PM_{10} in 2015. The EEA's air quality database consists of a multi-annual time series of air quality measurement data and calculated statistics for a number of air pollutants. For this evaluation background rural,

Table 2
Description of activity sectors used by EMEP and corresponding proxy applied for the downscaling.

GNFR name (ω)	GNFR usual name	Ground surface fraction (F in %)	Description	Proxy (φ)
GNFR1	A_PublicPower	0.25	Public electricity and heat production	ind
GNFR2	B_Industry	97	Petroleum refining, Manufacture of solid fuels and other energy industries	ind
GNFR3	C_OtherStationaryComb	100	Commercial/ military/ institutional/ residential Stationary combustion	res
GNFR4	D_Fugitive	100	Fugitive emissions in Industries	ind
GNFR5	E_Solvents	100	Solvent use, coating, chemical production	ind
GNFR6	F_RoadTransport	100	Road transport including tyres and brakes emissions: Passenger, Heavy Duty, Light Duty, Moped	tra
GNFR7	G_Shipping	100	National navigation including inland waterways	har
GNFR8	H_Aviation	100	Domestic and International aviation	avi
GNFR9	I_Offroad	100	Railways, off road in Agriculture, Forestry, Fishing and Industrial activities	off
GNFR10	J_Waste	41	Waste incineration, sewage, cremation, biological treatments	ind
GNFR11	K_AgriLivestock	100	Manure management – dairy cattle (beef, swine, poultry, etc …)	cro
GNFR12	L_AgriOther	100	Fertilizer spreading, field burning, other farm operations, uses of pesticides	cro

peri-urban and urban stations are selected. The calculated statistics are: Bias, RMSE and correlation, as well as the MQI - Model Quality Indicator (JRC, 2022; Kushta et al., 2019). For detailed description of the statistical indicators see Appendix B.

As displayed in Table 3 and Fig. 2 the downscaling method leads to an overall improvement in terms of statistics at the European level for most pollutants. Looking at individual countries the improvement of error statistics remains low in the supplementary data of Appendix C (Figs. S1–S6). The improvement is usually larger in terms of bias which is improved from about 1 to 1.5 μg m^{-3} for NO_2 and PM in urban areas. However, on annual average all statistics improve if we consider all type of stations. In general the correlation for NO_2 in urban areas slightly

Table 3
Overall statistics in terms of correlation (spatial), bias (μg m^{-3}), Root Mean Square Errors (μg m^{-3}) and Model Quality Indicator (MQI) between the LR and HR with downscaling for NO_2, PM_{10} and $PM_{2.5}$. Italic-bold character highlight the best performance.

Pollutant	Error statistics	LR	HR	Number of stations
NO_2	Cor.	0.687	***0.699***	1195
	Bias (μg m^{-3})	−8.16	***−7.49***	
	RMSE (μg m^{-3})	10.84	***10.28***	
	MQI	0.907	***0.833***	
PM_{10}	Cor.	0.485	***0.485***	1439
	Bias (μg m^{-3})	−10.73	***−10.51***	
	RMSE (μg m^{-3})	15.01	***14.85***	
	MQI	1.399	***1.372***	
$PM_{2.5}$	Cor.	0.652	***0.656***	763
	Bias (μg m^{-3})	−4.38	***−4.24***	
	RMSE (μg m^{-3})	6.59	***6.47***	
	MQI	0.400	***0.387***	

improved. To obtain a better improvement, an increase of the spatial resolution of emissions should be accompanied by an improvement of the resolution of meteorology, which is in line with findings of other studies (Baertsch-Ritter et al., 2004; Fenech et al., 2018; Jiang et al., 2020; Mircea et al., 2016). At last, it is important to observe that rural concentrations are very slightly influenced since the methodology mainly targets an improvement over urbanized and industrialized areas. Finally the bias improvement leads to improve the performances on MQI. Even if the improvement exists it remains low. As already been observed by (Colette et al., 2014) at the European scale with a fine scale simulation with a CTM over Europe at 2 km the correlation can even be deteriorated if the emission inventory is too inaccurate. Adding a more detailed top-down description of emission variability can also introduce a noisy signal which can deteriorate the realism of a simulation based on physical processes. The choice of proxy is probably crucial and can be improved in further developments or other applications.

Figs. 3 and 4 show the effect of the downscaling methodology on concentration maps over two regions in Europe. Particularly for NO_2, cities and roads appear on the HR maps (see also Fig. S7 in supplementary data of Appendix C over the North of Italy). Over the seas, no gains are obtained because we do not have implemented a proxy at 30 s arc for shipping routes, the only difference is due to the interpolation. Regardless of the pollutant, our methodology clearly improves results on urban areas. For $PM_{2.5}$, additional details appear at fine resolution close to Lyon in France with small cities appearing in the Functional Urban Area. However, also shown in Fig. S8 over the North of Italy, the impact of downscaling over areas affected by PM high concentrations the improvement is less visible compared to NO_2 since PM is driven by large scale processes.

4. Conclusion

The proposed proxy-based downscaling approach leads to increasing the pollutant fraction that is directly related to the local emissions. Its application leads to improved concentration maps where details appear clearly in vicinity of the sources (close to cities, industries and major roads). This improvement could be used for instance to better assess population exposure to air pollution.

When a HR emission inventory is available, the downscaling proxy is straightforwardly the HR emission dataset which can be aggregated at LR resolution to simulate air pollutant concentrations. Unfortunately, this case is not the most frequent, implying to downscale the LR emissions with a proxy-based approach (*e.g.* land-use and other ancillary data). Note that this approach can lead to some inconsistencies if proxies are not coherent with the LR emission inventory sectors. Our application belong to the second case. It highlights the added value of the downscaling in better estimating concentration fields.

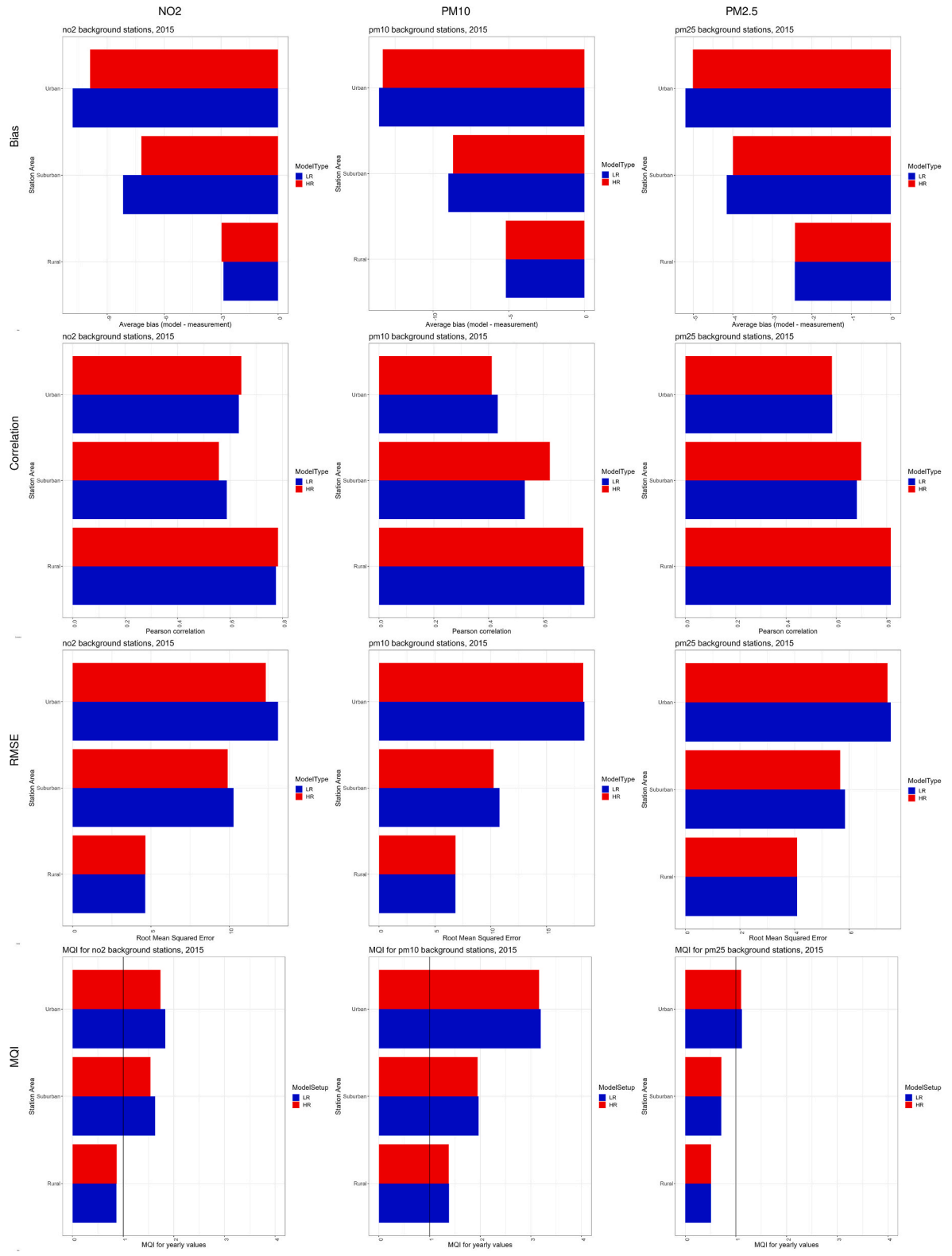

Fig. 2. Averaged performances of HR (red) versus LR (blue) simulations for NO_2, PM_{10} and $PM_{2.5}$ annual concentrations in terms of bias (μg m^{-3}), correlation (spatial) and Root Mean Square Errors (μg m^{-3}). The MQI is also added to see the impact of a highest resolution on the quality of models to support the Air quality directive.

One of the main limitations come from the secondary fractions which are interpolated at coarse grid level, the assumption being that the formation of these species is governed by slow processes (larger time scales than those related to the transport from one coarse grid cell to another). Therefore, the current downscaling procedure might be less effective for very coarse grid cells. On the other hand, the proxy-based downscaling procedure relies on the assumption that the pollutant concentration of interest mostly depends on local precursor emissions, so that a direct relation must exist between the pollutant and its emitted precursor. This assumption also depends on the chosen resolution and

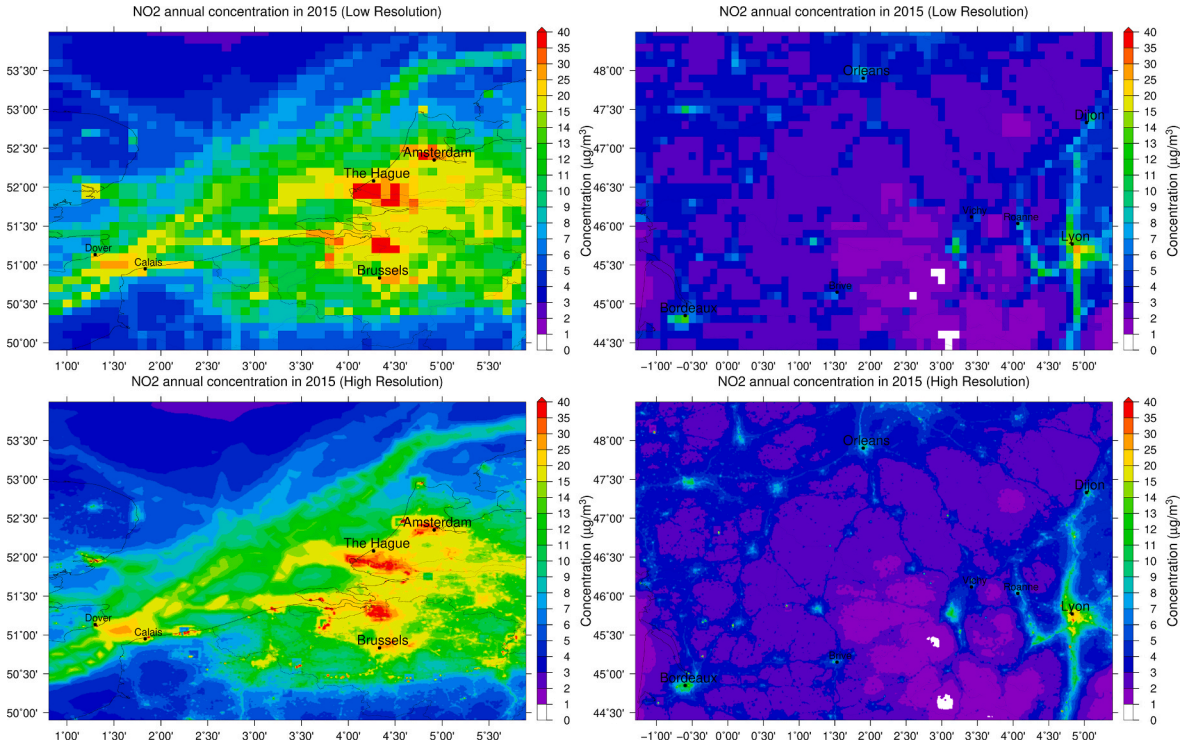

Fig. 3. Impact of the improvement from LR (top) to HR (bottom) resolution over the BeNeLux (left panel) and the south of France (right panel) for NO_2 annual mean concentrations.

would not work well if a too fine resolution is selected. The quality of the downscaling depends on the quality of the full modelling systems, so that *e.g.* if a LR simulation overestimates urban concentrations the resulting downscaled will increase this overestimation but still improving the spatial correlation if the resulting HR emission inventory is of good quality.

The methodology has been evaluated for all background rural, urban and peri urban stations for NO_2, PM_{10} and $PM_{2.5}$ in Europe. The bias improves in most parts of Europe, the spatial correlation is not affected although for NO_2 the HR spatial correlation is lower. The code runs fast and takes about 30 s for one pollutant to downscale a LR simulation field on a standard machine under a Linux OS - Intel(R) Xeon(R) Platinum 8168 CPU @ 2.70 GHz. For a given pollutant, a 90 Mbytes *netcdf* file is produced in our case. A by-product of our methodology is to provide a HR emission inventory detailed by activity sectors based on proxies.

As a perspective of this work, this post-processing modelling methodology will also be evaluated with a direct simulation at 0.01° resolution with the same modelling EMEP set-up at 0.1° to evaluate the capacity of this method to mimic a HR model simulation with all chemistry and physics processes on board. Also, the implementation of the mean wind direction to create a fast python module to create an asymmetric Gaussian kernel will be investigated to account for a more realistic spatial pattern of primary pollutants dispersion.

Credit author statement

Bertrand Bessagnet: Conceptualization; Data curation; Formal analysis; Investigation; Methodology; Software; Visualization; Roles/ Writing – original draft; Writing – Review & Editing.

Enrico Pisoni: Project administration, Conceptualization, Investigation, Software, Review & Editing.

Philippe Thunis: Project administration, Conceptualization, Investigation, Review & Editing.

Laurent Létinois: Software; Review & Editing.

Alexander de Meij: Data curation, Review & Editing.

Software and data availability

The main dataset and software are available. The scripts which create the proxy file in netcdf are available on request.

Name of the software: *downscaler*.

Developers: Bertrand Bessagnet, Enrico Pisoni, Alexander de Meij, Laurent Létinois, Philippe Thunis.

Contact information: bertrand.bessagnet@ec.europa.eu.

Year first available: 2022.

Program language: Python and Shell.

Cost: free.

Software availability

https://zenodo.org/record/7407932.

Program size: 186 Mb.

Funding

This research did not receive any specific grant from funding agencies in the public, commercial, or not-for-profit sectors.

Declaration of competing interest

The authors declare that they have no known competing financial interests or personal relationships that could have appeared to influence the work reported in this paper.

Data availability

The softawre and data are available at https://zenodo.org/record/7407932

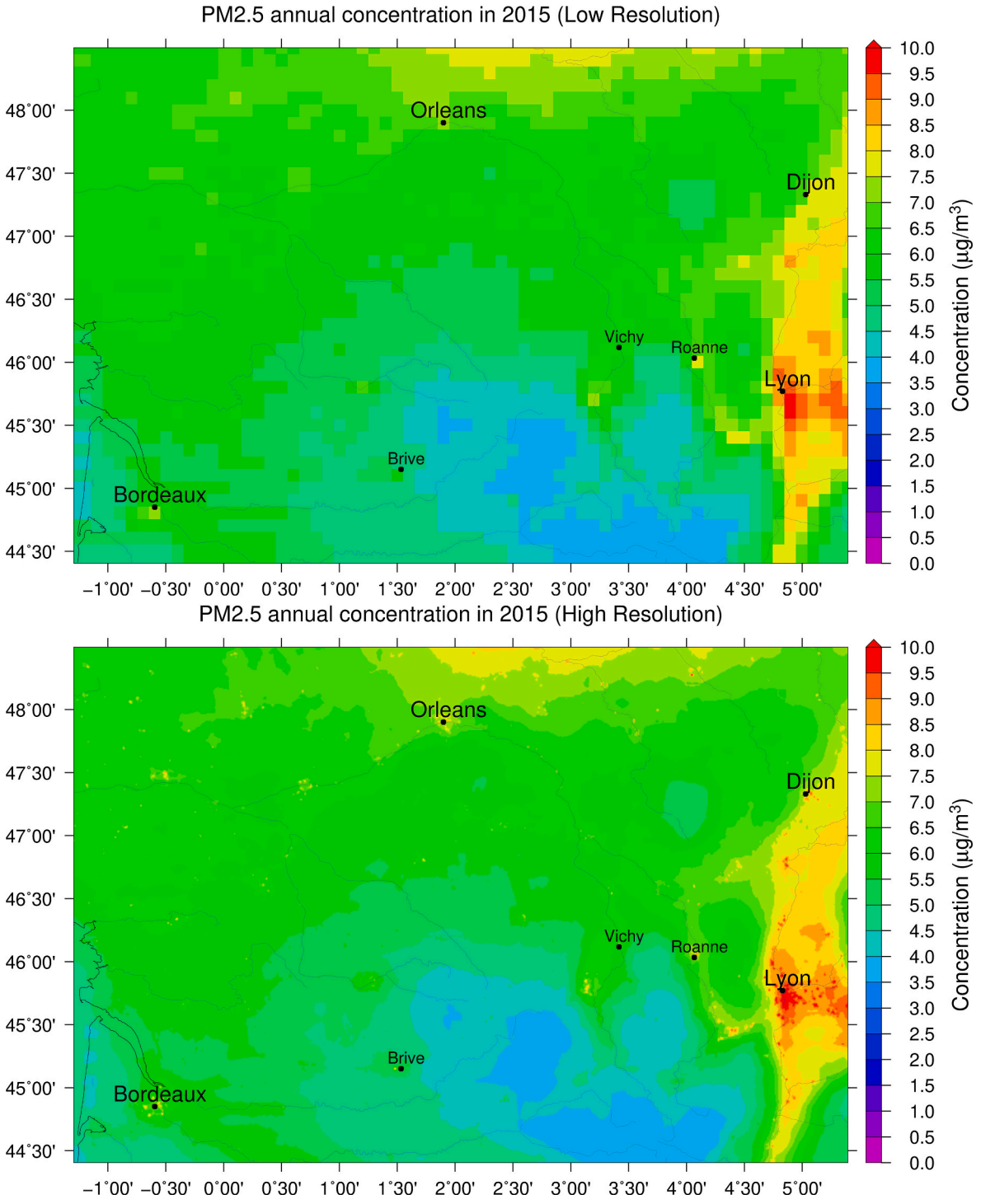

Fig. 4. Impact of the improvement from low (LR) to high (HR) resolution over the South of France for $PM_{2.5}$ annual mean concentrations.

Appendix A

A.1 Detailed description of the Algorithms

Here below a definition of each variable is provided. Capital letters for indices and variables refer to the LRG (Low Resolution Grid) while lower cases are reserved to the HRG (High Resolution Grid).

(I,J): grid cell coordinates of the LRG (I for longitude, J for latitude).
N_x, N_y: number of longitude and latitude indexes of the LRG grid, respectively.
(i,j): grid cell coordinates of the HRG (i for longitude, j for latitude).
n_x, n_y: number of longitude and latitude indexes of the HRG grid, respectively
nsx: scaling factor on longitude (integer) for downscaling
nsy: scaling factor on latitude (integer) for downscaling.
C: pollutant concentration over the LRG from the LR simulation
c: pollutant concentration over the HRG.
E: pollutant precursor emission over the LRG (Ton per grid cell).
e: pollutant precursor emission over the HRG (Ton per grid cell).
F: fraction of ground surface emission
p,s: indices for primary and non primary fractions (secondary and natural) of the pollutant concentration, respectively
r: index for the corresponding precursor emission.
X: virtual primary concentration in a coarse grid influenced for the correspondent emission of the cell evaluate by a box model.
ω: index for activity sectors
φ: associated proxy to the activity sector
Θ: value of 1 to count fine grid cells in a coarse grid cell
Γ: contribution (fraction between 0 and 1) of the primary fraction due to the cell emission itself.
σ: sigma parameter (in grid index unit) of the Gaussian filter (σ^b correspond to a class/bin *b*).
χ: ratio of the fine to the mother coarse mesh emissions of the precursor

The primary concentration with star * exponent represents its value based on the downscaling with the proxy -based approach. The "∼" accentuation sign is the result of a classic interpolation for a given concentration on the HRG, it corresponds here to a simple linear interpolation from the closest LRG concentration (selecting the four LRG grid points surrounding the HRG grid cell centre). The main algorithm is presented in equations (1)–(4).

The entire concentration C is decomposed in its primary and "non primary" (secondary fraction, naturals sources) for PM. For NO_2 we assume that the "non primary" fraction does not exist, however, natural and agricultural NO emissions exists but cannot be isolated in our calculations. This assumption could lead to overestimate the urban concentration of NO_2 in urban areas.

First, we estimate the fraction Γ as detailed in equations (1) and (2) as the fraction of primary fraction influenced by the given coarse cell out of the total primary concentration accounting for the influence of the regional transport from neighbouring cells. According to (Bessagnet et al., 2019), for a given cell *(I,J)*, the concentration *X* of a primary fraction due only to its local precursor emission *E* at the cell is estimated on a yearly average under neutral conditions, as:

$$X \cong \sqrt{\frac{\sqrt{\delta x \times \delta y}}{8ku}} \times E \tag{1}$$

E: emission flux of the precursor pollutant (μg m^{-2} s^{-1})
k: vertical eddy diffusion coefficient of the given cell (m^2 s^{-1})
u: wind speed of the given cell (m s^{-1})
δx: x axis dimension of the cell (m)
δy: y axis dimension of the cell (m)

Each pollutant is associated to a precursor pollutant *r* linked to the primary pollutant *p*: NOx for NO_2, PPM10 for the primary fraction of PM_{10} and PPM2.5 for the primary fraction of $PM_{2.5}$. For NO_2, an implicit assumption is that NOx emission is mostly converted in NO_2 concentrations for our scales using equation (1). In other words, given a "primary" precursor emissions we try to evaluate what should be the concentrations resulting from the emission in the cell due to only this emission at the cell thanks to a box model without chemistry. This "virtual" concentration X is used to calculate the fraction of the primary fraction which come from outside the cell.

It comes to calculate Γ over the coarse grid:

$$\Gamma_{I,J} = \frac{\sqrt{\frac{\sqrt{\delta x \times \delta y}}{8ku}} \times E_{I,J}}{C_{I,J}} \tag{2}$$

Γ is uniform over the coarse grid and is applied later in the algorithm for all fine cells (i,j) belonging to a coarse grid cell (I,J).

Second, the concentration c at fine scale is computed as the sum of (i) the fraction Γ from equation (2) of the primary component of C downscaled over the HRG, (ii) the "non primary" fraction as well as the remaining fraction $(1-\Gamma)$ of the primary component simply interpolated from the LRG to the HRG. The downscaled value of the primary fraction is afterwards diffused using a Gaussian filtering approach according a methodology described later. The downscaled proxy-based concentrations with proxy $c_{i,j}^{*,p}$ is proportional to the interpolated coarse concentrations ratio $\chi_{i,j}^{p\to r}$ which is the fraction of fine cell emission of the corresponding coarse cell emission. A minimum value is set to the minimum value of all coarse concentrations interpolated over the entire domain to avoid values equal to zero. A multi-gaussian filtering technique $Filter_\sigma$ (see details in the following appendix A.2) is applied to diffuse the downscaled concentrations according to the annual mean meteorological conditions for the given cell.

Two cases are identified: (a) we have access to a fine grid emission inventory and this ratio is directly computed on the basis of the HRG emission inventory; (b) only the emissions are available on the LRG and a preliminary downscaling of the emission inventory is required using adequate activity specific proxies φ associated to each given activity sector ω. This emission ratio is then multiplied by the total number of fine cells within a mother coarse grid cell $\sum_{i,j\in(I,J)}\Theta$ (equation (3)).

$$
\begin{aligned}
C_{I,J} &= C_{I,J}{}^{p} + C_{I,J}{}^{s} \\
\tilde{c}_{i,j}{}^{s} &= interp\left(C_{I,J}{}^{s}\right) \\
\tilde{c}_{i,j}{}^{p} &= interp\left(C_{I,J}{}^{p}\right) \quad : linear\ interpolation\ from\ LRG\ to\ HRG \\
c_{i,j} &= \overbrace{c_{i,j}{}^{p}}^{primary} + \overbrace{\left(1-\Gamma_{I,J_{i,j\in(I,J)}}\right)\times \tilde{c}_{i,j}{}^{p}}^{remaining\ primary} + \overbrace{\tilde{c}_{i,j}{}^{s}}^{non\ primary} \\
&\downarrow \\
c_{i,j}{}^{p} &= Filter_\sigma\left(c_{i,j}^{*,p}\right) \\
with \quad c_{i,j}^{*,p} &= max\left(\Gamma_{I,J_{i,j\in(I,J)}}\times \tilde{c}_{i,j}{}^{p}\times \chi_{i,j}^{p\to r}\times \sum_{i,j\in(I,J)}\Theta\ ; min_{\substack{1\le i\le n_x\\ 1\le j\le n_y}}\left(\tilde{c}_{i,j}{}^{p}\right)\right) \\
and\ \Theta &= 1 \\
\chi_{i,j}^{p\to r} &= \frac{\sum_\omega e_{i,j}^{\omega,r}}{\sum_{i,j\in(I,J)}\sum_\omega e_{i,j}^{\omega,r}}
\end{aligned}
\tag{3}
$$

If the emission ratio $\chi_{i,j}^{p\to r}$ requires the use of proxy to downscale the LR emission inventory (case (b) discussed before as it is the case in our application), we must first calculate an activity specific proxy defined as the ratio between its HR value and the sum of all values within a mother coarse grid cell as detailed in Eq. (4) Actually, any real positive number can be assigned to this ratio $\delta_{i,j}^{\omega\to\varphi}$ because *in fine* $Y_{i,j}^{\omega\to\varphi}$ is normalized by the coarse grid sum over the coarse grid $\sum_{i,j\in(I,J)}\delta_{i,j}^{\omega\to\varphi}$. If the sum $\sum_{i,j\in(I,J)}\delta_{i,j}^{\omega\to\varphi}$ is equal to zero we assign a uniform value to $Y_{i,j}^{\omega\to\varphi}$ e.g. 0.01 if 100 fine grid cells are present in the coarse grid cell.

$$
\begin{aligned}
&if\ e_{i,j}^{\omega,r}\ does\ not\ exist, \forall i,j\in(I,J) \quad : \quad e_{i,j}^{\omega,r} = Y_{i,j}^{\omega\to\varphi}\times E_{I,J}^{\omega,r}\times F^{\omega} \\
&\qquad if\ \sum_{i,j\in(I,J)}\delta_{i,j}^{\omega\to\varphi}\neq 0 \quad : \quad Y_{i,j}^{\omega\to\varphi} = \frac{\delta_{i,j}^{\omega\to\varphi}}{\sum_{i,j\in(I,J)}\delta_{i,j}^{\omega\to\varphi}} \\
&if\ \sum_{i,j\in(I,J)}\delta_{i,j}^{\omega\to\varphi} = 0 \quad : \quad Y_{i,j}^{\omega\to\varphi} = \frac{\Theta}{\sum_{i,j\in(I,J)}\Theta}\ with\ \Theta = 1 \\
&\qquad \forall\omega \sum_{i,j\in(I,J)} Y_{i,j}^{\omega\to\varphi} = 1
\end{aligned}
\tag{4}
$$

The emission $e_{i,j}^{\omega,r}$ for each grid cell by activity sector ω is actually the ground fraction F^{ω} below 184 m (Table 2) according to the vertical distribution used in the EMEP model. The scheme in Fig. A1 visualizes the downscaling procedure for a regular coarse grid mesh of 0.1° resolution with scaling factors of 10 both in latitude and longitude. This part of the code is written in *Python* (Van Rossum and Drake, 2009), the use of a regular HRG which perfectly matches the LRG with uniform scaling factors allows a very fast computing thanks to the *numpy* and *scipy* libraries (Harris et al., 2020; Virtanen et al., 2020).

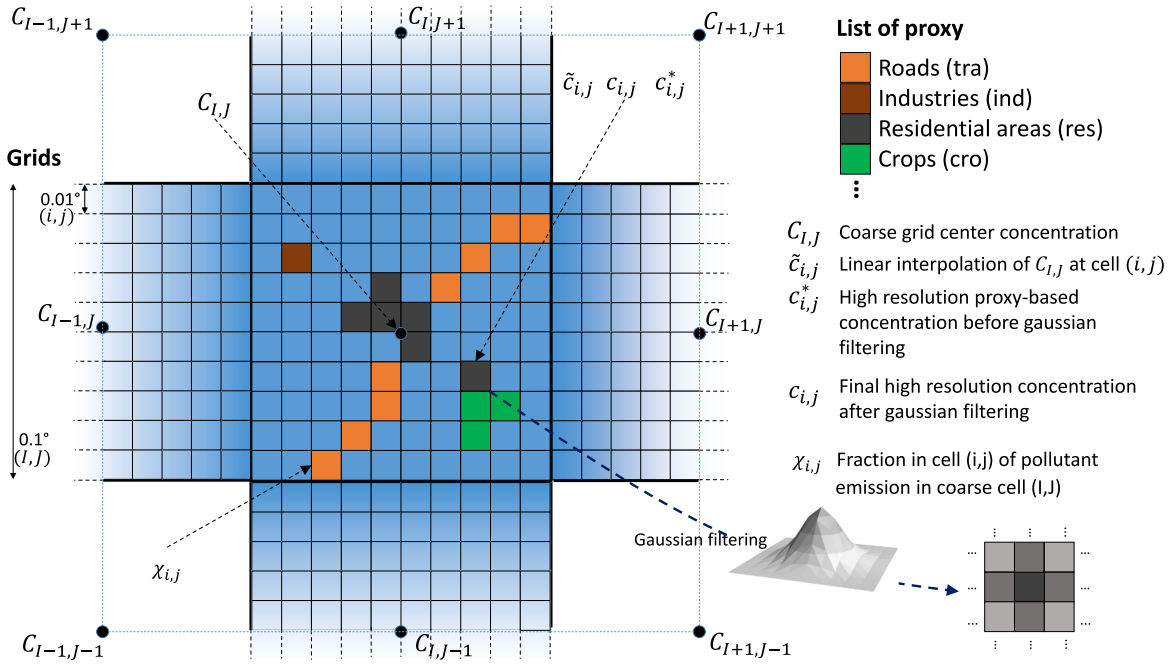

Fig. A.1. Visual description of the downscaling methodology applied to grid resolutions corresponding to our application example. The hatched cell is the grid of interest, in this example the bilinear interpolation at this point requires the coarse grid cell concentrations $C_{I,J}$, $C_{I+1,J}$, $C_{I+1,J-1}$ and $C_{I,J-1}$. Here we consider nsx × nsy = 10 × 10 for the example.

A.2 The Gaussian filtering technique Filter$_\sigma$

To account for atmospheric dispersion processes between high resolution grid cells, and obtain a more realistic field of primary concentrations c, we use here a Gaussian dispersion equation and apply it using the *scipy* python library which offers the possibility to smooth a 2D array using a Gaussian approach. This type of filtering is appropriate since Gaussian equations correspond to analytical solutions of the dispersion in air pollution modelling. A 2D Gaussian filter G for a given σ (grid index unit) is defined as:

$$c_{i,j} = \sum_{k=1}^{n_x} \sum_{l=1}^{n_y} c^*_{k,l} G^{\sigma}_{k,l}(i-k, j-l) \tag{5}$$

$$G^{\sigma}_{k,l}(i_k, j_l) = \frac{1}{2\pi {\sigma_{k,l}}^2} e^{-\frac{{i_k}^2 + {j_l}^2}{2{\sigma_{k,l}}^2}}$$

$$\sum_{i_k=-w}^{i_k=+w} \sum_{j_l=-w}^{j_l=+w} G^{\sigma}_{k,l}(i_k, j_l) \cong 1$$

i_k and j_l are the new coordinate system on both axes from cell (k,l) of the HRG grid corresponding to the new origin $i_k = 0 ; j_l = 0$. σ depends on dispersion conditions and has to be evaluated first for each grid cell. w is the size of the footprint with the width $(2 \bullet w + 1)$ of the regular squared windows centered over the cell (k,l) where the central cell is diffused in 2D. This windows width is defined by the python procedure using a specific input parameter and a dependency with σ. The computation is then optimized to avoid useless calculations over the full grid since G quickly tends to 0 when $\frac{{i_k}^2+{j_l}^2}{2{\sigma_{k,l}}^2}$ becomes very large. An increase of σ implies an increase of the computation time. Actually, the resulting diffused concentration by the Gaussian filter at cell (i,j) is c as:

$$c = \frac{1}{2\pi\sigma^2} c^* \tag{6}$$

Then, by using equations (1) and (6) which provides in a stationary regime the concentration produced by the cell emission, σ^2 is estimated for a fine grid cell as:

$$\sigma^2 = \frac{1}{2\pi} \sqrt{\frac{8ku}{\sqrt{\delta x \times \delta y}}} \times \frac{c^*}{e} \tag{7}$$

In practice, to save computing time and benefit from existing compact libraries, we simplify the use of a Gaussian filtering by using only 20 classes b of sigma σ^b (discrete scale of σ) with a step of 0.5 defined by the list in equation (7) to apply the Gaussian filtering approach. The step and the number of classes can be changed but these values provide a satisfactory results in our case after several tests.

$$
\begin{aligned}
&if\ \sigma < 0.5 \quad : \sigma^b = 0\\
&if\ 0.5 \le \sigma < 1 : \sigma^b = 0.5\\
&if\ 1 \le \sigma < 1.5 : \sigma^b = 1\\
&\ldots\\
&if\ \sigma \ge 10 : \sigma^b = 10
\end{aligned}
\tag{8}
$$

The filtering technique of *scipy* called scipy.ndimage.gaussian_filter (Virtanen et al., 2020) is then applied for the HRG by class of σ (called σ^b) as previously defined and the final concentrations is the sum over all classes b as:

$$Filter_\sigma\left(c_{i,j}^{*,p}\right) = \sum_b \left[\sum_{k=1}^{n_x} \sum_{l=1}^{n_y} c_{k,l}^{*,p} G_{k,l}^{\sigma^b}(i-k, j-l) \right] \tag{9}$$

This approach is therefore fully additive.

Appendix B

Error statistics used to evaluate model performance (M and O refer respectively with Model and Observations data, and N is the number of observations). U_{95} is the 95th percentile measurement uncertainty of the observed concentration level, and β is the coefficient that scales the proportionality of the bias to the measurement uncertainty (Kushta et al., 2019).

Bias	$Bias = (\overline{M} - \overline{O})$ with $\overline{M} = \frac{1}{N}\sum_{i=1}^{N} M_i$ and $\overline{O} = \frac{1}{N}\sum_{i=1}^{N} O_i$
Root Mean Square Error	$RMSE = \sqrt{\frac{1}{N}\sum_{i=1}^{N}(M_i - O_i)^2}$
Correlation Coefficient	$R = \left(\sum_{i=1}^{N}(M_i - \overline{M})(O_i - \overline{O})\right) / \left(\sqrt{\sum_{i=1}^{N}(M_i - \overline{M})^2 \times \sum_{i=1}^{N}(O_i - \overline{O})^2}\right)$
Model Quality Index	$MQI_i = \frac{\lvert M_i - O_i \rvert}{\beta U_{95}(O_i)}$ *with* $\beta = 2$

Appendix. C: Supplementary data

Supplementary data to this article can be found online at https://doi.org/10.1016/j.envsoft.2023.105692.

References

AIRBASE, 2022. Air quality e-reporting (AQ e-reporting) — European environment agency [WWW Document]. URL. https://www.eea.europa.eu/data-and-maps/data/aqereporting-9. (Accessed 18 June 2022).

Baertsch-Ritter, N., Keller, J., Dommen, J., Prevot, A.S.H., 2004. Effects of various meteorological conditions and spatial emission resolutions on the ozone concentration and ROG/NOx; limitation in the Milan area (I). Atmos. Chem. Phys. 4, 423–438. https://doi.org/10.5194/acp-4-423-2004.

Beauchamp, M., Bessagnet, B., de Fouquet, C., Malherbe, L., Meleux, F., Ung, A., 2018. An additive geostatistical model for mixing total and partial PM10 observations with CHIMERE rCTM. Atmos. Environ. 189, 61–79.

Beauchamp, M., Fouquet, C. de, Malherbe, L., 2017. Dealing with non-stationarity through explanatory variables in kriging-based air quality maps. Spatial Statistics 22, 18–46. https://doi.org/10.1016/j.spasta.2017.08.003.

Bessagnet, B., Beauchamp, M., Menut, L., Fablet, R., Pisoni, E., Thunis, P., 2021. Deep learning techniques applied to super-resolution chemistry transport modeling for operational uses. Environ. Res. Commun. 3, 085001 https://doi.org/10.1088/2515-7620/ac17f7.

Bessagnet, B., Couvidat, F., Lemaire, V., 2019. A statistical physics approach to perform fast highly-resolved air quality simulations ? A new step towards the meta-modelling of chemistry transport models. Environ. Model. Software 116, 100–109.

Bessagnet, B., Pirovano, G., Mircea, M., Cuvelier, C., Aulinger, A., Calori, G., Ciarelli, G., Manders, A., Stern, R., Tsyro, S., García Vivanco, M., Thunis, P., Pay, M.-T., Colette, A., Couvidat, F., Meleux, F., Rouïl, L., Ung, A., Aksoyoglu, S., Baldasano, J. M., Bieser, J., Briganti, G., Cappelletti, A., D'Isidoro, M., Finardi, S., Kranenburg, R., Silibello, C., Carnevale, C., Aas, W., Dupont, J.-C., Fagerli, H., Gonzalez, L., Menut, L., Prévôt, A.S.H., Roberts, P., White, L., 2016. Presentation of the EURODELTA III intercomparison exercise – evaluation of the chemistry transport models' performance on criteria pollutants and joint analysis with meteorology. Atmos. Chem. Phys. 16, 12667–12701. https://doi.org/10.5194/acp-16-12667-2016.

Bieser, J., Aulinger, A., Matthias, V., Quante, M., Denier Van Der Gon, H.A.C., 2011. Vertical emission profiles for Europe based on plume rise calculations. Environ. Pollut. 159, 2935–2946. https://doi.org/10.1016/j.envpol.2011.04.030.

Binkowski, F.S., Roselle, S.J., 2003. Models-3 community multiscale air quality (CMAQ) model aerosol component 1. Model description. J. Geophys. Res. 108, 2001JD001409 https://doi.org/10.1029/2001JD001409.

Binkowski, F.S., Shankar, U., 1995. The regional particulate matter model: 1. Model description and preliminary results. J. Geophys. Res. 100, 26191 https://doi.org/10.1029/95JD02093.

Broxton, P.D., Zeng, X., Sulla-Menashe, D., Troch, P.A., 2014. A global land cover climatology using MODIS data. J. Appl. Meteorol. Climatol. 53, 1593–1605. https://doi.org/10.1175/JAMC-D-13-0270.1.

CEIP, 2019. Reporting instructions [WWW Document]. URL. https://www.ceip.at/fileadmin/inhalte/ceip/00_pdf_other/2019/06122019_conversiontablereportingcodes_.xlsx. (Accessed 29 June 2021).

Ciarelli, G., Aksoyoglu, S., El Haddad, I., Bruns, E.A., Crippa, M., Poulain, L., Äijälä, M., Carbone, S., Freney, E., O'Dowd, C., Baltensperger, U., Prévôt, A.S.H., 2017. Modelling winter organic aerosol at the European scale with CAMx: evaluation and source apportionment with a VBS parameterization based on novel wood burning smog chamber experiments. Atmos. Chem. Phys. 17, 7653–7669. https://doi.org/10.5194/acp-17-7653-2017.

CIESIN, 2018. Gridded population of the world, version 4 (GPWv4): population density adjusted to match 2015 revision UN WPP country totals. Revision 11. https://doi.org/10.7927/H4F47M65.

CLC, 2020. CLC 2018 — Copernicus land monitoring Service [WWW Document]. URL. https://land.copernicus.eu/pan-european/corine-land-cover/clc2018. (Accessed 18 June 2022).

Colette, A., Bessagnet, B., Meleux, F., Terrenoire, E., Rouïl, L., 2014. Frontiers in air quality modelling. Geosci. Model Dev. (GMD) 7, 203–210. https://doi.org/10.5194/gmd-7-203-2014.

Denby, B.R., Gauss, M., Wind, P., Mu, Q., Grøtting Wærsted, E., Fagerli, H., Valdebenito, A., Klein, H., 2020. Description of the uEMEP_v5 downscaling approach for the EMEP MSC-W chemistry transport model. Geosci. Model Dev. (GMD) 13, 6303–6323. https://doi.org/10.5194/gmd-13-6303-2020.

Dong, C., Loy, C.C., He, K., Tang, X., 2014. Learning a deep convolutional Network for image super-resolution. In: Fleet, D., Pajdla, T., Schiele, B., Tuytelaars, T. (Eds.), Computer Vision – ECCV 2014. Springer International Publishing, Cham, pp. 184–199. https://doi.org/10.1007/978-3-319-10593-2_13.

EEA, 2019. Air Quality in Europe: 2019 Report. Publications Office, LU.

Fenech, S., Doherty, R.M., Heaviside, C., Vardoulakis, S., Macintyre, H.L., O'Connor, F. M., 2018. The influence of model spatial resolution on simulated ozone and fine particulate matter for Europe: implications for health impact assessments. Atmos. Chem. Phys. 18, 5765–5784. https://doi.org/10.5194/acp-18-5765-2018.

Feranec, J., Soukup, T., Hazeu, G., Jaffrain, G. (Eds.), 2016. European Landscape Dynamics, 0 ed. CRC Press. https://doi.org/10.1201/9781315372860.

GDAL, 2022. GDAL software. https://doi.org/10.5281/ZENODO.5884351.

Harris, C.R., Millman, K.J., van der Walt, S.J., Gommers, R., Virtanen, P., Cournapeau, D., Wieser, E., Taylor, J., Berg, S., Smith, N.J., Kern, R., Picus, M., Hoyer, S., van Kerkwijk, M.H., Brett, M., Haldane, A., del Río, J.F., Wiebe, M., Peterson, P., Gérard-Marchant, P., Sheppard, K., Reddy, T., Weckesser, W., Abbasi, H., Gohlke, C., Oliphant, T.E., 2020. Array programming with NumPy. Nature 585, 357–362. https://doi.org/10.1038/s41586-020-2649-2.

Jiang, L., Bessagnet, B., Meleux, F., Tognet, F., Couvidat, F., 2020. Impact of physics parameterizations on high-resolution air quality simulations over the Paris region. Atmosphere 11.

JRC, 2022. FAIRMODE Guidance Document on Modelling Quality Objectives and Benchmarking: Version 3.3. Publications Office, LU. https://doi.org/10.2760/41988.

Kushta, J., Georgiou, G.K., Proestos, Y., Christoudias, T., Thunis, P., Savvides, C., Papadopoulos, C., Lelieveld, J., 2019. Evaluation of EU air quality standards through modeling and the FAIRMODE benchmarking methodology. Air Qual Atmos Health 12, 73–86. https://doi.org/10.1007/s11869-018-0631-z.

LeCun, Y., Bengio, Y., Hinton, G., 2015. Deep learning. Nature 521, 436–444. https://doi.org/10.1038/nature14539.

Lin, C., Wang, Y., Ooka, R., Flageul, C., Kim, Y., Kikumoto, H., Wang, Z., Sartelet, K., 2022. Modelling of street-scale pollutant dispersion by coupled simulation of chemical reaction, aerosol dynamics, and CFD (preprint). Dynamics/Atmospheric Modelling/Troposphere/Physics (physical properties and processes). https://doi.org/10.5194/acp-2022-365.

Mailler, S., Menut, L., Khvorostyanov, D., Valari, M., Couvidat, F., Siour, G., Turquety, S., Briant, R., Tuccella, P., Bessagnet, B., Colette, A., Létinois, L., Markakis, K., Meleux, F., 2017. CHIMERE-2017: from urban to hemispheric chemistry-transport modeling. Geosci. Model Dev. (GMD) 10, 2397–2423.

Malherbe, L., Meleux, A.U.F., Bessagnet, B., Steyn, D., Builtjes, P., Timmermans, R., 2014. A statistical approach to improve air quality forecasts in the PREV'AIR system. Air Pollution Modeling and Its Application 205–209.

Mareckova, K., Pinteris, M., Ullrich, B., Wankmueller, R., Gaisbauer, S., 2019. Review of Emission Data Reported under the LRTAP Convention and the NEC Directive Stage 1 and 2 Review Status of Gridded and LPS Data (EMEP Report No. 4/2019). Umweltbundesamt GmbH, Vienna, Austria.

Menut, L., Bessagnet, B., Briant, R., Cholakian, A., Couvidat, F., Mailler, S., Pennel, R., Siour, G., Tuccella, P., Turquety, S., Valari, M., 2021. The CHIMERE v2020r1 online chemistry-transport model. Geosci. Model Dev. (GMD) 14, 6781–6811. https://doi.org/10.5194/gmd-14-6781-2021.

Mircea, M., Grigoras, G., D'Isidoro, M., Righini, G., Adani, M., Briganti, G., Ciancarella, L., Cappelletti, A., Calori, G., Cionni, I., Cremona, G., Finardi, S., Larsen, B.R., Pace, G., Perrino, C., Piersanti, A., Silibello, C., Vitali, L., Zanini, G., 2016. Impact of grid resolution on aerosol predictions: a case study over Italy. Aerosol Air Qual. Res. 16, 1253–1267. https://doi.org/10.4209/aaqr.2015.02.0058.

Mu, Q., Denby, B.R., Wærsted, E.G., Fagerli, H., 2022. Downscaling of air pollutants in Europe using uEMEP_v6. Geosci. Model Dev. (GMD) 15, 449–465. https://doi.org/10.5194/gmd-15-449-2022.

Owens, R., Hewson, T., 2018. ECMWF forecast user guide. https://doi.org/10.21957/M1CS7H.

Paolella, D.A., Tessum, C.W., Adams, P.J., Apte, J.S., Chambliss, S., Hill, J., Muller, N.Z., Marshall, J.D., 2018. Effect of model spatial resolution on estimates of fine particulate matter exposure and exposure disparities in the United States. Environ. Sci. Technol. Lett. 5, 436–441. https://doi.org/10.1021/acs.estlett.8b00279.

Ramacher, M.O.P., Kakouri, A., Speyer, O., Feldner, J., Karl, M., Timmermans, R., Denier van der Gon, H., Kuenen, J., Gerasopoulos, E., Athanasopoulou, E., 2021. The UrbEm hybrid method to derive high-resolution emissions for city-scale air quality modeling. Atmosphere 12, 1404. https://doi.org/10.3390/atmos12111404.

Schaap, M., Cuvelier, C., Hendriks, C., Bessagnet, B., Baldasano, J.M., Colette, A., Thunis, P., Karam, D., Fagerli, H., Graff, A., Kranenburg, R., Nyiri, A., Pay, M.T., Rouïl, L., Schulz, M., Simpson, D., Stern, R., Terrenoire, E., Wind, P., 2015. Performance of European chemistry transport models as function of horizontal resolution. Atmos. Environ. 112, 90–105.

Simpson, D., Benedictow, A., Berge, H., Bergström, R., Emberson, L.D., Fagerli, H., Flechard, C.R., Hayman, G.D., Gauss, M., Jonson, J.E., Jenkin, M.E., Nyíri, A., Richter, C., Semeena, V.S., Tsyro, S., Tuovinen, J.-P., Valdebenito, Á., Wind, P., 2012. The EMEP MSC-W chemical transport model – technical description. Atmos. Chem. Phys. 12, 7825–7865. https://doi.org/10.5194/acp-12-7825-2012.

Sokhi, R.S., Moussiopoulos, N., Baklanov, A., Bartzis, J., Coll, I., Finardi, S., Friedrich, R., Geels, C., Grönholm, T., Halenka, T., Ketzel, M., Maragkidou, A., Matthias, V., Moldanova, J., Ntziachristos, L., Schäfer, K., Suppan, P., Tsegas, G., Carmichael, G., Franco, V., Hanna, S., Jalkanen, J.-P., Velders, G.J.M., Kukkonen, J., 2022. Advances in air quality research – current and emerging challenges. Atmos. Chem. Phys. 22, 4615–4703. https://doi.org/10.5194/acp-22-4615-2022.

Sorek-Hamer, M., Von Pohle, M., Sahasrabhojanee, A., Akbari Asanjan, A., Deardorff, E., Suel, E., Lingenfelter, V., Das, K., Oza, N.C., Ezzati, M., Brauer, M., 2022. A deep learning approach for meter-scale air quality estimation in urban environments using very high-spatial-resolution satellite imagery. Atmosphere 13, 696. https://doi.org/10.3390/atmos13050696.

Terrenoire, E., Bessagnet, B., Rouïl, L., Tognet, F., Pirovano, G., Létinois, L., Beauchamp, M., Colette, A., Thunis, P., Amann, M., Menut, L., 2015. High-resolution air quality simulation over Europe with the chemistry transport model CHIMERE. Geosci. Model Dev. (GMD) 8, 21–42.

Van Rossum, G., Drake, F.L., 2009. Python 3 Reference Manual. CreateSpace, Scotts Valley, CA.

Virtanen, P., Gommers, R., Oliphant, T.E., Haberland, M., Reddy, T., Cournapeau, D., Burovski, E., Peterson, P., Weckesser, W., Bright, J., van der Walt, S.J., Brett, M., Wilson, J., Millman, K.J., Mayorov, N., Nelson, A.R.J., Jones, E., Kern, R., Larson, E., Carey, C.J., Polat, İ., Feng, Y., Moore, E.W., VanderPlas, J., Laxalde, D., Perktold, J., Cimrman, R., Henriksen, I., Quintero, E.A., Harris, C.R., Archibald, A.M., Ribeiro, A. H., Pedregosa, F., van Mulbregt, P., Vijaykumar, A., Bardelli, A.P., Rothberg, A., Hilboll, A., Kloeckner, A., Scopatz, A., Lee, A., Rokem, A., Woods, C.N., Fulton, C., Masson, C., Häggström, C., Fitzgerald, C., Nicholson, D.A., Hagen, D.R., Pasechnik, D.V., Olivetti, E., Martin, E., Wieser, E., Silva, F., Lenders, F., Wilhelm, F., Young, G., Price, G.A., Ingold, G.-L., Allen, G.E., Lee, G.R., Audren, H., Probst, I., Dietrich, J.P., Silterra, J., Webber, J.T., Slavič, J., Nothman, J., Buchner, J., Kulick, J., Schönberger, J.L., de Miranda Cardoso, J.V., Reimer, J., Harrington, J., Rodríguez, J.L.C., Nunez-Iglesias, J., Kuczynski, J., Tritz, K., Thoma, M., Newville, M., Kümmerer, M., Bolingbroke, M., Tartre, M., Pak, M., Smith, N.J., Nowaczyk, N., Shebanov, N., Pavlyk, O., Brodtkorb, P.A., Lee, P., McGibbon, R.T., Feldbauer, R., Lewis, S., Tygier, S., Sievert, S., Vigna, S., Peterson, S., More, S., Pudlik, T., Oshima, T., Pingel, T.J., Robitaille, T.P., Spura, T., Jones, T.R., Cera, T., Leslie, T., Zito, T., Krauss, T., Upadhyay, U., Halchenko, Y.O., Vázquez-Baeza, Y., 2020. SciPy 1.0: fundamental algorithms for scientific computing in Python. Nat. Methods 17, 261–272. https://doi.org/10.1038/s41592-019-0686-2.

Xing, J., Zheng, S., Ding, D., Kelly, J.T., Wang, S., Li, S., Qin, T., Ma, M., Dong, Z., Jang, C., Zhu, Y., Zheng, H., Ren, L., Liu, T.-Y., Hao, J., 2020. Deep learning for prediction of the air quality response to emission changes. Environ. Sci. Technol. 54, 8589–8600. https://doi.org/10.1021/acs.est.0c02923.